High-resolution observations of eight 3CR compact steep-spectrum radio sources

R. E. Spencer, R. T. Schilizzi, C. Fanti, R. Fanti, R. Fanti, P. Parma, W. J. M. van Breugel, T. Venturi, T. W. B. Muxlow and Nan Rendong

- ¹University of Manchester, Nuffield Radio Astronomy Laboratories, Jodrell Bank, Macclesfield, Cheshire SK11 9DL
- ²Netherlands Foundation for Research in Astronomy, Radiosterrenwacht Dwingeloo, Postbus 2, 7990 AA, The Netherlands
- ³Dipartimento di Astronomia, Via Zamboni 33, 40126 Bologna, Italy
- ⁴Istituto di Radioastronomia del CNR, Via Irnerio 46, 40126 Bologna, Italy
- ⁵Institute of Geophysics and Planetary Physics, Lawrence Livermore National Laboratory, PO Box 808, L-413, Livermore, CA 94550, USA
- ⁶Beijing Observatory, Academia Sinica, Beijing, PR China

Accepted 1991 January 10. Received 1991 January 10; in original form 1990 October 3

SUMMARY

We present high-resolution observations carried out at 18-cm wavelength with MERLIN and the European VLBI Network (EVN) on eight compact steep-spectrum (CSS) sources from the 3CR catalogue (3C43, 186, 190, 286, 299, 318, 346, 454). The typical resolution achieved on maps made with combined data is \leq 30 mas. The relationships between compact features on these maps with low-brightness extended regions seen in the MERLIN data alone can be found. Prominent jets were found in seven sources, enabling us to discuss the properties of jets for the 3CR sample of CSS sources in general. The jet opening angle is similar to that in large-scale powerful radio sources, but several jets show pronounced curvature and bending perhaps indictive of strong interactions with an interstellar medium. The jet/counter-jet brightness ratios are consistent with moderate ($\beta \geq$ 0.7) Doppler boosting.

1 INTRODUCTION

Compact steep spectrum sources are high-luminosity extragalactic radio sources with steep radio spectra ($\alpha > 0.5$, $S \sim$ $v^{-\alpha}$) at frequencies ≥ 1 GHz and small linear size. Our sample (Fanti et al. 1985) consists of the sources from the revised 3CR sample (Jenkins, Pooley & Riley 1977) with $P_{178} > 10^{26} \text{ W} \text{ Hz}^{-1}$ that at the time of selection were believed to have at least 80 per cent of their flux density from within a region of projected linear size of $\leq 10 \text{ kpc} (H_0 = 100 \text{ m})$ km s⁻¹ Mpc⁻¹, $q_0 = 1$). This paper concludes the first part of research begun in 1981 aimed at mapping the 3CR CSS's with resolution at 1.7 GHz of ≤100 pc, which therefore requires the angular resolution of very long baseline interferometer (VLBI) techniques. The 26-member sample of the 3CR CSS's is given in Table 1, together with references to the relevant papers where details on the sources can be found. Only one source from Table 1 has not yet been observed with VLBI (3C305.1) but, from what is known from other observations [5 GHz MERLIN, Akujor et al. 1991; 15 GHz very large array (VLA), van Breugel et al., in preparation], the lack of 1.7-GHz VLBI data does not affect our discussion. Note that the low observing frequency of the 3CR catalogue selects against CSS's smaller than ~ 1 kpc (Spencer *et al.* 1989).

This paper presents maps of eight sources (3C43, 186, 190, 286, 299, 318, 346, 454). We include combined MERLIN + EVN maps at 5 GHz for 3C286, maps from 1.7-GHz MERLIN data and 1.5-GHz VLA data for 3C346 (where the linear resolution is similar to that on the other sources due to its low redshift), and combined MERLIN+EVN maps at 1.7 GHz on the remaining sources. The use of combined data, together with modern techniques of data analysis which correct for telescope gain and phase errors for both arrays simultaneously (see e.g. Muxlow et al. 1988) enables higher dynamic range maps to be produced than achievable with VLBI alone. This method brings out features in the sources which enable relationships between high-brightness knots and low-brightness jets and lobes to be found. 6-cm MERLIN maps of six of the sources discussed here (3C43, 286, 299, 318, 346, 454) are presented by Akujor et al. (1991).

A statistical analysis of the properties of the CCS's and a discussion of their nature as a possible evolutionary stage of

Table 1. Compact steep-spectrum sources from the 3CR catalogue.

		-							-
Name	z	Id(m-v)	S178 : Jy	Size "	α h.fr.	logP178 W/Hz	LS k pc	Моз	r Ref
3C43 0127+23	1.46	Q(20.0)	11.6	2.6	. 71	28.4	9.4	T	1,5,6
3C48 0134+32	0.37	Q(16.2)	55.0	1.3	. 82	27.9	2.1	С	5,6,8,9,10
3C49 0138+13	0.62	G(22.0)	10.3	1.0	. 89	27.6	3.6	D	2, 4, 5, 6
3C67 0221+27	0.31	G(18.0)	10.0	2.5	. 93	27.0	6.8	D	2,5,6,8
3C119 0429+41	0.41	Q(20.0)	15.7	. 2	. 65	27.4	0.9	J	3,5,6,8
3C138 0518+16	0.76	Q(17.9)	22.2	. 8	. 65	28.1	2.9	J	4,6,8,5
3C147 0538+49	0.55	Q(16.9)	60.5	. 7	. 83	28.3	2.4	T	5,6,8,9
3C186 0740+38	1.06	Q(17.6)	14.1	2.2	1.08	28.2	8.2	T	1,7
3C190 0758+14	1.2	Q(20.0)	15.0	4.0	. 89	28.3	14.1	T	1,6
3C216 0906+43	0.67	Q(18.5)	20.2	8.0	. 78	28.0	28.8	T	6,11
3C237 1005+07	Ó. 88	G(21)	20.9	1.2	. 91	28.3	4.5	D	2,5,6
3C241 1019+22	1.62	G(>22)	11.6	1.2	1.28	28.5	2.8	D	2,5,6
3C268.3 1203+64	0.37	G(19.0)	10.7	1.3	. 97	27.2	3.9	D	2,5,6,8
3C286 1328+30	0.85	Q(17.3)	25.0	3.8	. 55	28.3	14.2	T	1,5,6,8
3C287 1328+27	1.06	Q(17.7)	16.3	. 1	. 63	28.3	0.4	J	2,4,6,8
3C298 1416+06	1.44	Q(16.8)	47.5	2.5	1.1	29.0	9.1	T	5,6
3C299 1419+41	0.37	G(19.5)	11.8	0.5	. 88	27.2	1.5	С	1,5,6,8
3C303. 1 1443+77	0.27	G(19.0)	8.1	2.0	1.07	26.8	5.0	D	2,5,6
3C305.1 1447+77	1.13	G(21.0)	4.6	2.8	. 96	28.0	9.0	D	5,6
3C309.1 1458+71	0.9	Q(16.8)	22.7	2.2	. 60	28.3	7.8	T	5,6,8,9
3C318 1517+20	0.75	G(20.3)	12.3	. 8	. 92	27.8	7.8	T	1,6
3C343 1634+62	0.99	Q(20.6)	12.4	. 25	5 .84	28. 1	0.7	С	2,6,8
3C343.1 1637+62	0.75	G(20.8)	11.5	. 38	3 . 99	27.8	1.3	D	2,5,6,8
3C346 1641+17	0.16	G(17.2)	10.9	11.0	. 65	26.5	19.6	D	1
3C380 1828+48	0.69	Q(16.8)	59.7	16.0	. 57	28.5	57.0	С	6,10
3C454 2249+18	1.76	Q(18.5)	11.6	.6	. 76	28.6	2.1	T	1,6,7

References: (1) This paper: (2) Fanti et al. (1985); (3) Fanti et al. (1986); (4) Fanti et al. (1989); (5) Spencer et al. (1989); (6) Pearson et al. (1985); (7) Cawthorne et al. (1986); (8) van Breugel et al. (1984); (9) Wilkinson et al. (1984a); (10) Wilkinson et al. (1984b); (11) Wilkinson et al. (1990); (12) Barthel et al. (1988).

the more extended radio sources are given by Spencer *et al.* (1989) and Fanti *et al.* (1990). We discuss some of the properties of jets in CSS sources in this paper.

Table 2. Observational data.

(1) source	(2) date	(3) VLBI network	(4) Rec mode	(5) beam (mas)	(6) pc/mas	Norm. Amin		(8) noise mTy/b	(9) dyn. r
3C 43	86272 82299	SLDBWJ	Mk2	24x22(58)	3.6	0.27	0.09	1.35	230
3C186	86269 82053	SLBWJ	Mk3	28x22(67)	3.7	0.18	0.04	0.15	320
3C190	88330 82056	SLBWJ	Mk3	28x25(64)	3.7	0.11	0.03	0.25	240
3C286+	87308 83238.		Mk2	10x8 (62)	3.7	0.66	0. 15	1.25	600
3C299	88332 82307	SLBWJ	Mk3	30x30(0)	3.0	0.10	0.02	0.45	150
3C318	87061 87317 82300		Mk2 Mk2	35x33(46)	3.7	0.37	0.18	0.65?	580
3C346	87227 83056	!	:	250x180(86)	1.8	\$0.44	0.09	0.45	400
3C454	86072 87059 82103	SWCD SLBWJZ	Mk2	24x22(32)	3.5	0.56	0.24	0.60	530

S=Onsala; L=Medicina; B=Effelsberg; W=Westerbork; J=Jodrell Bank (Lovell or Mk2); D=Defford; C=Cambridge; Z=Torun. (+) at 6 cm, (\$) min/max in MERLIN, (!) VLA and MERLIN observations. All sources had also MERLIN observations. 3C186 and 3C190 had 'extended' MERLIN coverage (i.e. Cambridge telescope added). COLUMN HEADINGS: (1) Source name; (2) Date of observations, in the form of year followed by day number; (3) Telescopes used for VLBI observations; (4) Recording mode used: Mk2 narrow bandwidth, Mk3 – wide bandwidth; (5) Smallest restoring beam sizes, position angle in brackets; (6) Scale on maps in pc mas -1; (7) Normalized fringe visibility at shortest and longest VLBI baselines; (8) rms noise level on the maps; (9) Dynamic range of the maps, peak brightness to lowest 'believable' contour.

2 OBSERVATIONS AND DATA REDUCTION

Observations were made using telescopes in the European VLBI network in the period 1986-88 (see Table 2). Each source was tracked for 10-12 hr and observations interleaved with three to four 30-min scans on calibration sources. Two sources, 3C318 and 3C454, were observed twice, since the first observation had partially failed. In both cases, however, the second observation was done with a different network of antennas, so that the two sets of data turned out to be complementary to each other. All sources were also observed with MERLIN (consisting of the Jodrell Bank, Tabley, Darnhall, Wardle, Knockin and Defford telescopes, with the occasional addition of the Cambridge 18-m telescope), at the same frequency, but different epochs (Table 2). The 3C43 observations included the Defford telescope in the VLBI network and for 3C454 both Defford and Cambridge were added. This provided extra baselines of intermediate length between MERLIN and the EVN, which were very useful for linking the two networks.

The VLBI signals were recorded with the standard Mk2 system with a 1.8-MHz bandwidth or with Mk3 and 28-MHz bandwidth, depending on the source strength. The Mk3 data were correlated in Bonn, and the Mk2 data either in Bonn or with the Caltech Block-II correlator. Coherent integration times of 1 or 2 min were chosen, depending on the source structure and intensity. The correlated flux density scale was

calibrated following Cohen et al. (1975), using 0235+164, 0Q208 and DA193. These sources are believed to be essentially unresolved at the various interferometer spacings. Their total flux densities were measured at Effelsberg and Westerbork during the observations. The internal consistency of the calibration factors for each of the baselines is generally better than 5 per cent. The MERLIN data were

calibrated using flux density and baseline calibrator sources as described by Spencer et al. (1989).

A quick impression of the complexity of the CSS structures can be obtained by examining column 7 in Table 2 where we have listed the normalized fringe visibilities at approximately the shortest and longest VLBI baselines (roughly 1 and $8 \text{ M}\lambda$ respectively at 1.7 GHz). Note that even

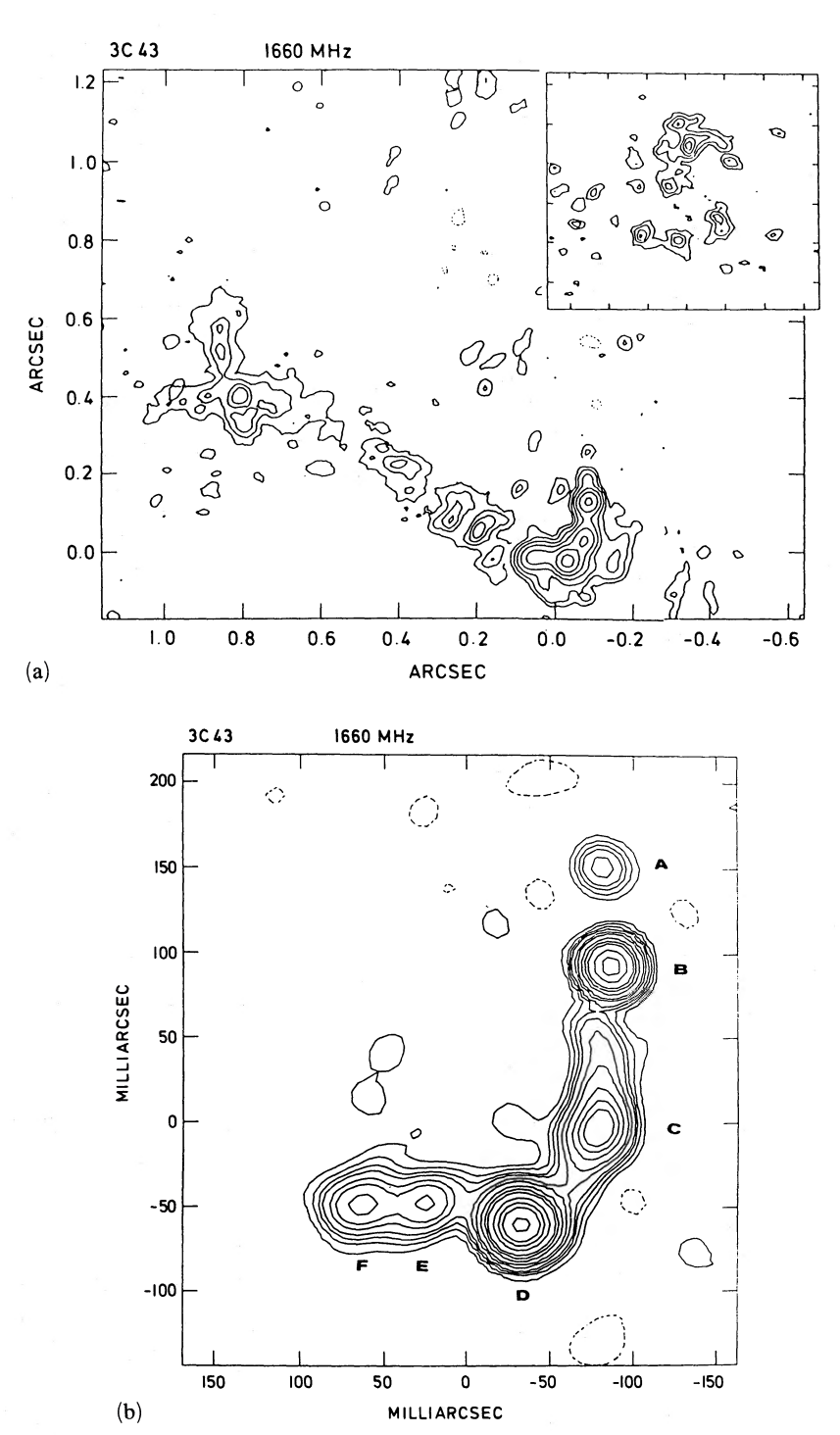


Figure 1. 3C43 (a) Combined EVN + MERLIN map. The beam size is 40×40 mas². The central component at (0,0) is contoured at -2.5, 5, 7.5, 10, 20, 40, 80, 160 and 320 mJy beam⁻¹; for the northern component, contours are 2, 3, 4, 5, 6 mJy beam⁻¹; for the eastern component and jet contours are -2.5, 2.5, 5, 7.5 and 10 mJy beam⁻¹. (b) EVN map. The beam size is 24×22 mas² (pa 58°); contours are at -6, 4, 8, 12, 16, 24, 32, 48, 64, 80, 120, 160, 200 and 280 mJy beam⁻¹.

on the shortest VLBI baselines the fringe visibilities hardly exceed 50 per cent, emphasizing the importance of the MERLIN data to fill in the gaps at short spacings and improve the mapping of these objects.

A careful matching of the flux density scales of MERLIN and EVN was made after comparison of the flux densities of the respective calibrator sources. After ensuring that the total flux densities of the sources had not varied between observing epochs, the MERLIN and VLBI data were combined to produce maps with a range in resolution and sensitivity. This was done to determine the optimal representation of small- and large-scale features in each of the sources. Nevertheless 5–10 per cent of the total flux density is missing in several maps.

For 3C43 and 3C286 we followed the usual procedures in VLBI map-making. First a preliminary model fitting of the visibility amplitudes was made to obtain a reliable starting model. Next we performed several iterations using the hybrid mapping technique, including CORTEL (Cornwell & Wilkinson 1981) for the self-calibration step. At a later stage the independently self-calibrated MERLIN data were added, and the reduction was continued using the National Radio Astronomy Observatory (NRAO) package AIPS, on the VAX computer in Bologna, which makes use of an Array Processor in the mapping and cleaning routines.

For the other sources we used the difference mapping algorithm (Cornwell & Wilkinson 1983) running under the OLAF system on the ALLIANT computer in Jodrell Bank. This allowed hybrid mapping to be undertaken on the combined set of EVN and MERLIN data in a controlled manner with continuous visual interaction between user and system such that spurious symmetrizations could be reduced to a minimum. We believe that such effects do not occur in our data. Having obtained a well-corrected data set, we used AIPS task MX to obtain an optimum deconvolution and map. For the source 3C346, with combined MERLIN and VLA data, we followed a different approach, as described in Section 3.7.

The maps of the various CSS sources are shown in Figs 1–8. Usually we display images of the same source at different resolution. The rms noise level (1σ) at some distance from the source and the dynamic range achieved (peak to rms noise ratio) in the high-resolution maps are given in Table 2. The synthesized beam size depends on the u-v coverage obtained. The typical resolution achieved at 1.7 GHz in the combined maps is of the order of 20–30 mas (Table 2).

We applied the following standard analysis to all of the sources.

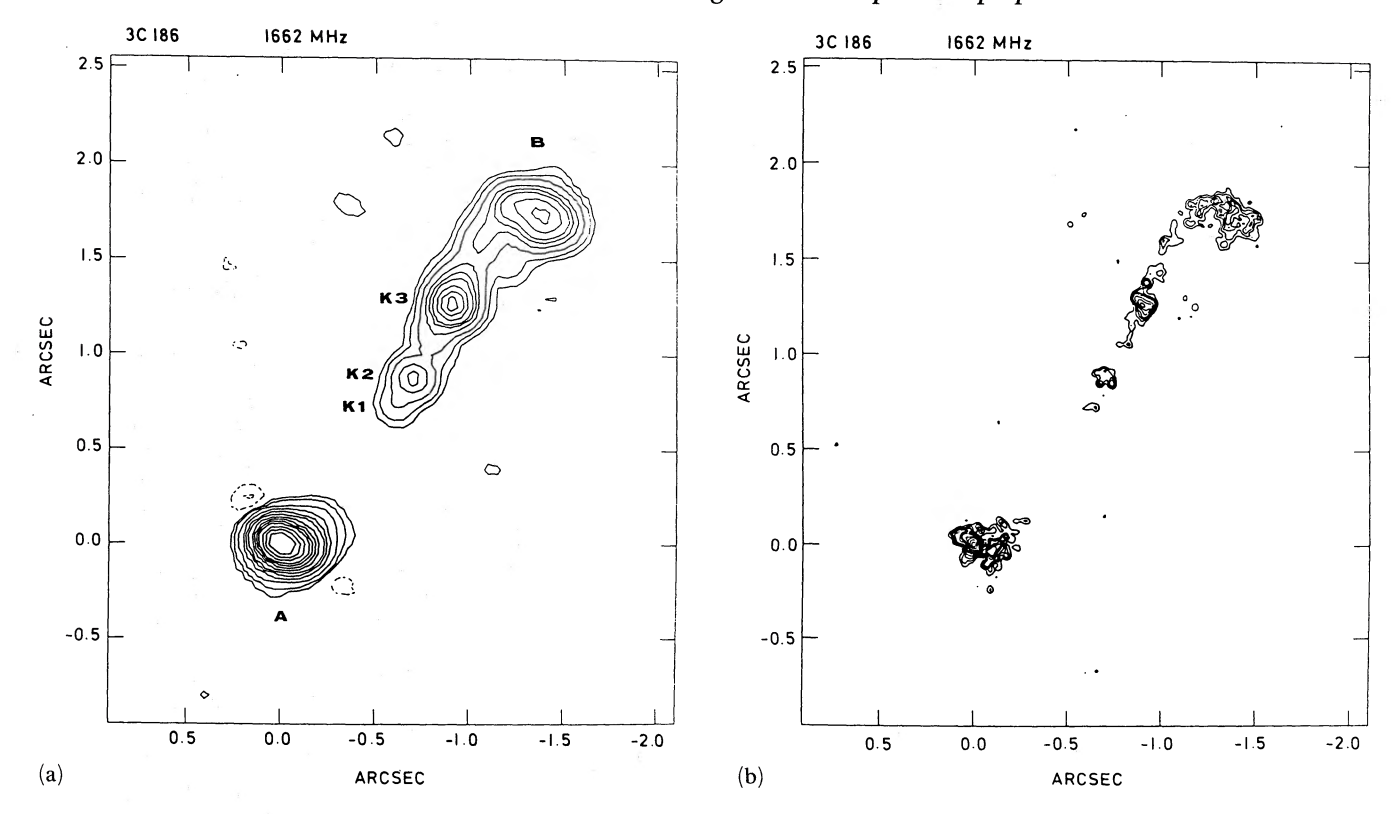
- (i) Gaussian models were fitted to clearly identifiable components to obtain diameters (HPW), deconvolved for the observing beam.
- (ii) Angular sizes were estimated from the lowest reliable contour when sources had complicated extended components and Gaussian fitting was not applicable. Note that this gives a size which is 1.5-2 times the half-power size in typical cases.
- (iii) The total flux density was obtained by integration over the source subcomponents. We consider this more reliable than the value given by the Gaussian fits since it is more sensitive to the extended low-brightness features on which high-brightness peaks are often superimposed.

(iv) When a 'jet' was present (see next Section) we produced one-dimensional brightness profiles perpendicular to the local jet orientation. These were fitted with a one-dimensional Gaussian. The derived FWHM, deconvolved for the

Table 3. Source parameters.

		F						
Source	Comp	S mJy	sep mas	pa dg	th1 mas	th2 mas	pa dg	Notes
3C 43	A B ext C D E	25 210 50 200 480 95 90	0 58 125 154 216 225 247	0 -176 180 178 167 152 144	<10 8 120 34 18 30 24	5 45 10 15 14	140 ~0 156 112 109 124	(1),*
St(Jy)	East Centr North	600 1720 170 2. 67	~940 0 ~2500	65 0 -23		- (2)	Ī.,	(2) (2)
Detay		2.01						
3C186	A k1 k2 k3 N-jet B	520 12 40 80 130 290	970 0 150 600 - 1250	138 0 -25 -25 - -36	350 - 93 85 725 460	250 - 65 48 100 320	- 60 34 -33	(3),* (3) (3) (3), (3),*
St(Jy)		1.1						
3C190 St(Jy)	A B C bridg D L1 L2	665 515 60 ~120 565 240 140 2.3	1660 1160 0 - 1030 ~600 ~2800	-125 -127 0 - 32 -25 -136	390 450 30 - 330 -	190 170 17 - 310 -	170 43 93 - 0 -	(4) (4) (4)
25204		4000		•		-		
3C286 St(Jy)	A B C D	4330 1120 110 ~700 6.95	0 32 73 25	0 -140 -137 52	14 22 18 34	7 10 12 28	45 49 90 50	•
3C299	A B C East	665 525 390 1840	0 230 370	0 -163 -163	180 140 150 750	120 90 70 200	20 0 23 20	(5),* (5),* (5),*
St (Jy)	ridge West ridge	640 2.52	-	-	900	150	10	•
3C318	A k1 k2 k3	710 90 580 155	565 120 0 165	-138 -142 0 33	350 85 34 90	230 30 15 35	60 6 40 8	•
St(Jy)	ext B	~300 ~70 2.19	480	- 40	460 750	80 325	40 140	(6),* (7),*
3C346	k1 k2 k3 jet W.h.sp A	175 210 165 ~350 50 ~1200	0 2130 3560 - 5630	0 80 70 - -108	65 150 480 - 960 7850	30 75 410 - 590 5500	69 80 55 - 70 125	(8) (9) (10),*
St(Jy)	В	~2000 3.40			7400	6500	70	(10),*
3C454 St(Jy)	k1 k2 k3 k4 A N.h.sp B C	610 220 260 40 200 23 80 80 65	0 90 135 187 500 495 335 115 270	0 -177 -176 -178 -23 -23 -126 5 -178	39 24 25 35 295 15 220 120	6 14 14 21 236 7 160 60 90	21 4 178 13 167 37 54 ~0	(11),* (11),* *
DC(Jy)		1.90						

St – source flux density from single dish mesurements * – diameter from the lowest believable contour; (1) – weak emission underlying C, between B and D; (2) – from map in Fig. 1(a); 'Centr' includes the bright jet (A to F); east includes weak jet beyond F and lobe; (3) – from map in Fig. 2(c); N-jet is the feature north of k3 merging into lobe B; (4) – from the map in Fig. 3b; 'bridge' refers to the extended emission, between C and B (flux of C excluded); (5) – A, B and C are part of east ridge; (6) – extended emission underlying knots in Fig. 6(b); (7) – from map in Fig. 6(a); (8) – jet underlying knots from k1 to k3; (9) – from Fig. 7(b); (10) – from map in Fig. 7(c), fine structures included; (11) – from map in Fig. 8(b).



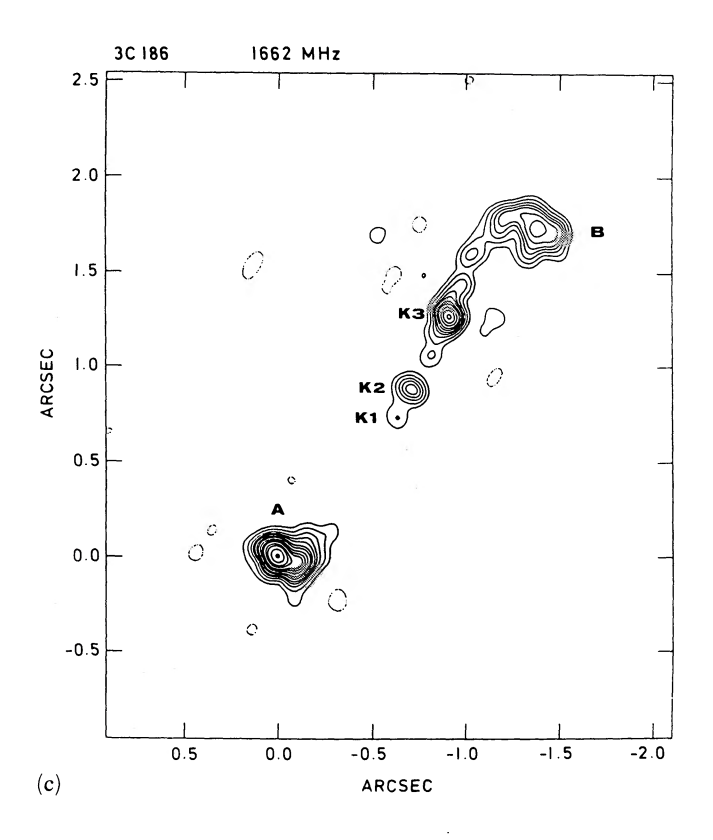


Figure 2. 3C186 (a) MERLIN map. The beam size is 162×132 mas² (pa 59°) and contours at -4, -2, 2, 4, 8, 16, 24, 32, 48, 64, 80, 96, 128, 160 and 200 mJy beam $^{-1}$; (b) Contour plot of the combined EVN + MERLIN map with levels at -2, 1, 2, 3, 4, 6, 8, 10, 15, 20, 30 and 40 mJy beam $^{-1}$. (c) Combined EVN + MERLIN map, convolved to a resolution of 84×84 mas² and contours at -2, 3, 6, 10, 14, 18, 24, 30, 40, 50, 60, 80, 100, 140 and 180 mJy beam $^{-1}$.

observing beam, was used to study the 'jet' opening angle, defined as the rate of increase of the jet FWHM as a function of the distance from the source core.

Table 3 gives the observed parameters for the sources and their various components, labelled as in the figures. Flux densities and sizes are derived from the most appropriate of the maps shown, usually the high-resolution map, unless specified otherwise (see notes). The total flux densities

reported are from WSRT mesurements, simultaneous with the VLBI observations, and are given for comparison.

3 DESCRIPTION OF THE SOURCES

3.1 3C43

At a resolution of a few tenths of an arcsec (Pearson, Perley & Readhead 1985; Spencer et al. 1989), the source shows a

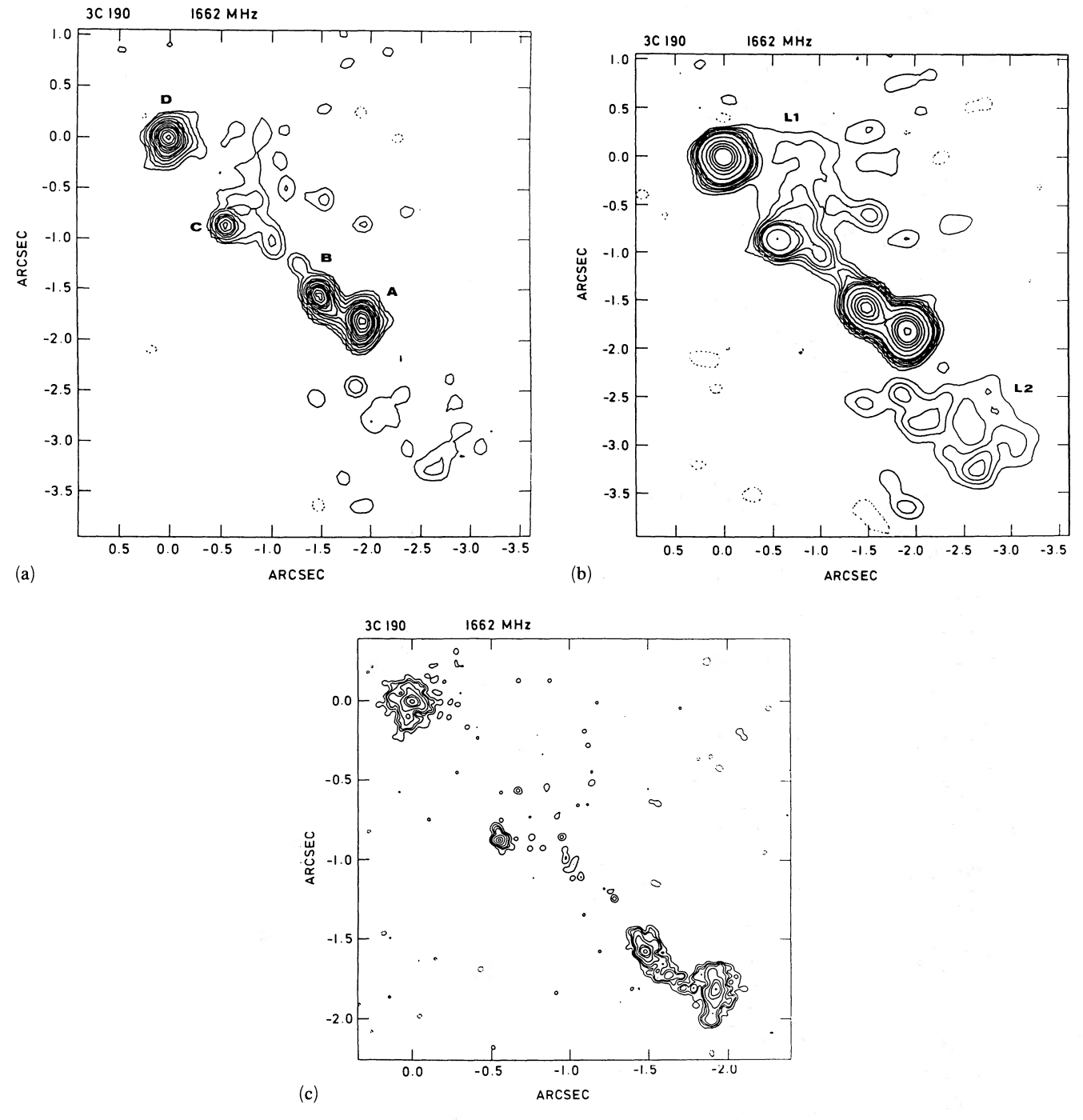


Figure 3. 3C190 (a) MERLIN map. The beam size is 144×128 mas² (pa 34°) with contours at -6, -3, 3, 6, 12, 24, 36, 48, 72, 96, 120, 144, 192, 240 and 300 mJy beam⁻¹. (b) MERLIN map convolved to a resolution of 230×200 (pa 66°), contours at -3, 3, 6, 9, 12, 18, 24, 30, 60, 120, 180, 240, 300 and 450 mJy beam⁻¹. (c) Combined EVN + MERLIN map. The beam size is 34×34 mas² and the contours are at -1.5, 1.5, 3, 4.5, 7.5, 15, 30, 45 and 75 mJy beam⁻¹.

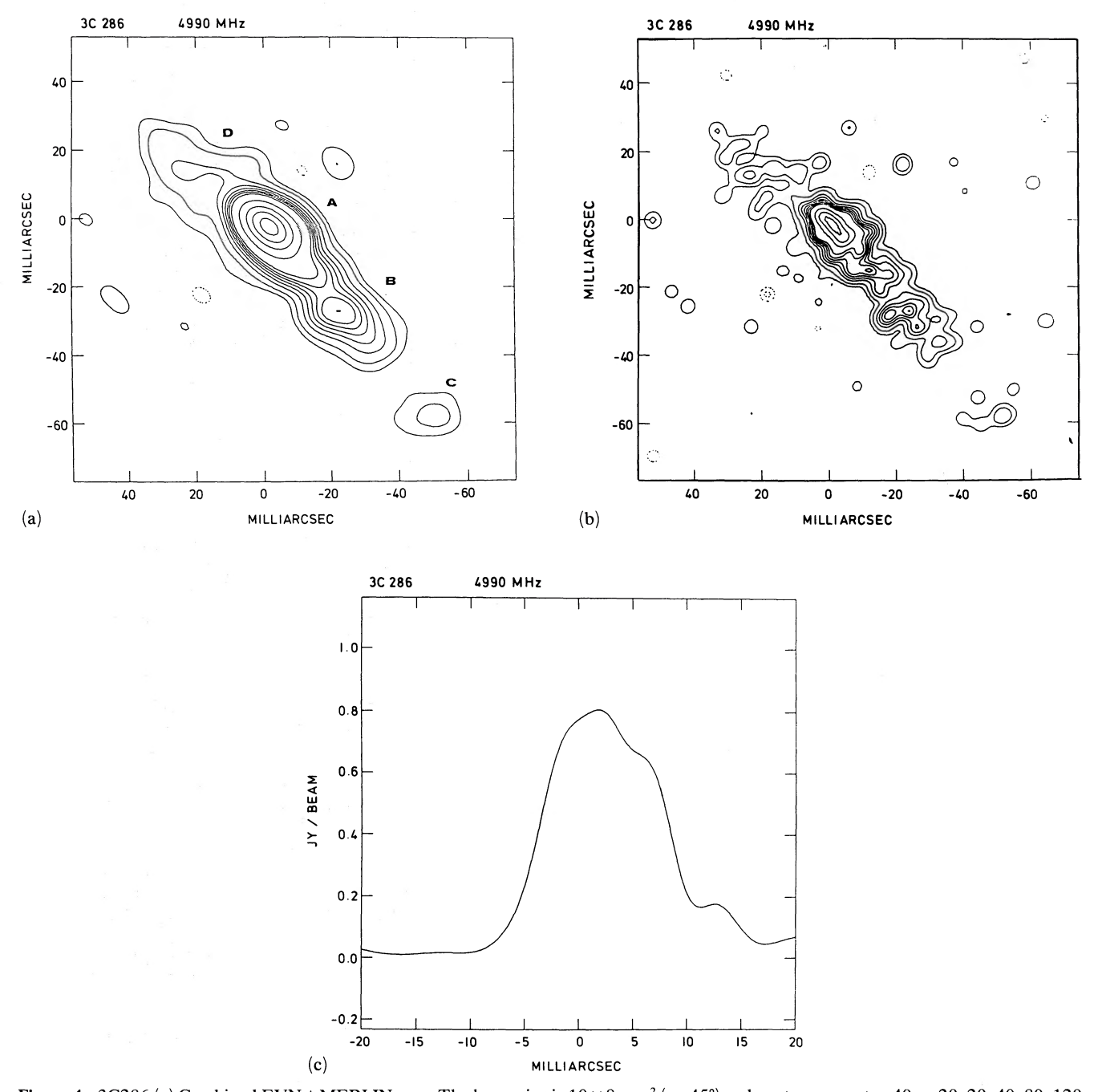


Figure 4. 3C286 (a) Combined EVN + MERLIN map. The beam size is 10×8 mas² (pa 45°) and contours are at -40, -20, 20, 40, 80, 120, 160, 200, 240, 300, 600, 1000, 1400 and 1800 mJy beam⁻¹. (b) Same map as (a), at the super-resolution of 4×4 mas² and levels are -20, -10, 10, 20, 40, 60, 80, 100, 120, 150, 300, 500 and 700 mJy beam⁻¹. (c) Surface brightness profile from map (b), along the jet axis.

markedly non-linear triple structure, with a central component lying close to the optical quasar (Pearson *et al.* 1985) and two outer lobes misaligned with the central component. The data available in the literature show that the outer lobes have a steep spectrum ($\alpha \sim 1.2$) in the frequency range of 1.7–15 GHz, while the central 'unresolved' component has a flatter spectrum ($\alpha \sim 0.65$). The spectral decomposition of the total emission shows that the flux density below 500 MHz is dominated by the lobe emission. This indicates that the spectrum of the central component may turn over below

 ~ 500 MHz. The MERLIN 6-cm map shows this component to be L-shaped (Akujor *et al.* 1991).

The three components can still be recognized in a higher resolution map of $40\times40~\text{mas}^2$ beamsize (Fig. 1a) obtained with the combined MERLIN+EVN networks, although the north-western component is just above the noise. Note that the three components are plotted with different contours, with the N component shown as an inset and the E jet component superimposed on the map. The central L-shaped component consists of a number of knots, located along a

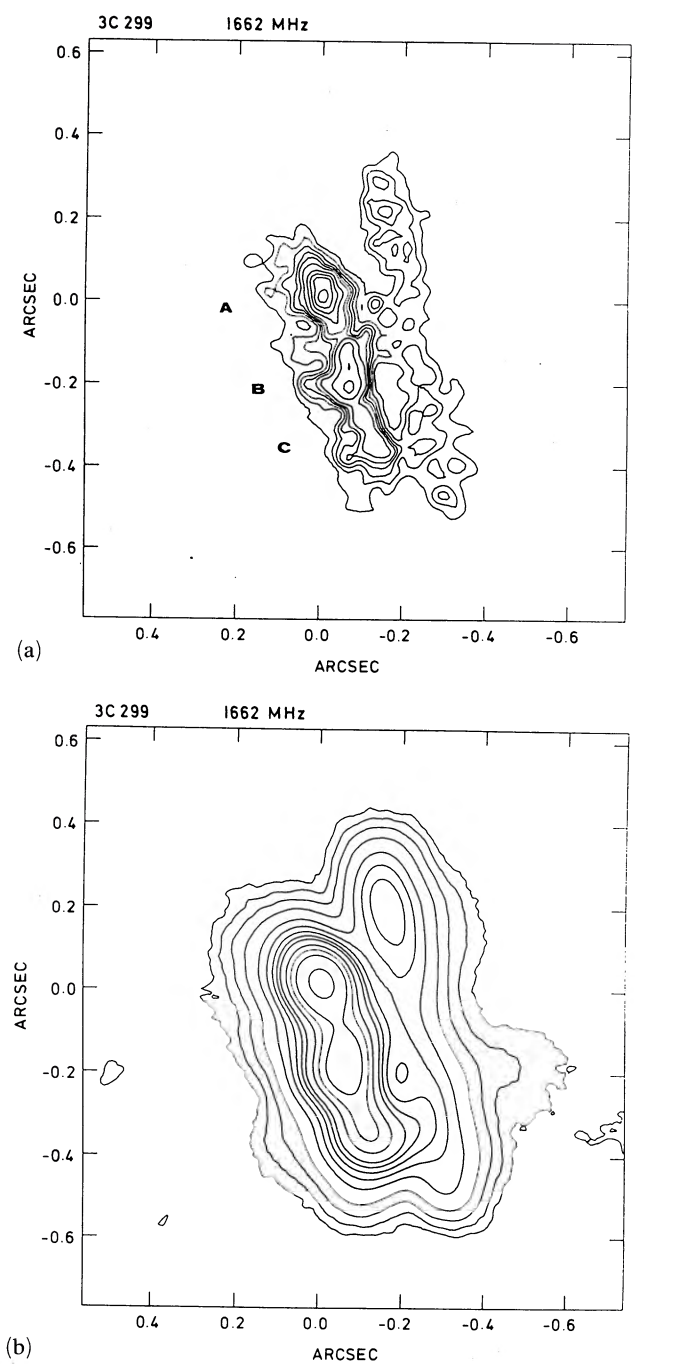


Figure 5. 3C299 (a) Combined EVN+MERLIN map. The beam size is 30×30 mas 2 and levels at -1, 3, 6, 9, 12, 15, 20, 30, 40, 50 and 60 mJy beam $^{-1}$. (b) Map convolved to a resolution of 100×100 mas 2 and levels at -4, -2, 2, 4, 8, 16, 32, 48, 64, 80, 96, 128, 160, 200 and 300 mJy beam $^{-1}$.

sharply bent line whose extremes point roughly to the outer lobes, and surrounded by lower brightness emission. The eastern lobe appears connected to this 'bright' jet by a low-brightness collimated structure ('faint jet'). About 7 per cent of the total flux density is missing in this map, probably in the more extended features (lobes).

In the EVN map of Fig. 1(b), at full resolution $(24 \times 22 \text{ mas}^2)$ only the central component is seen, but its knotty structure is shown in greater detail. The low-brightness emis-

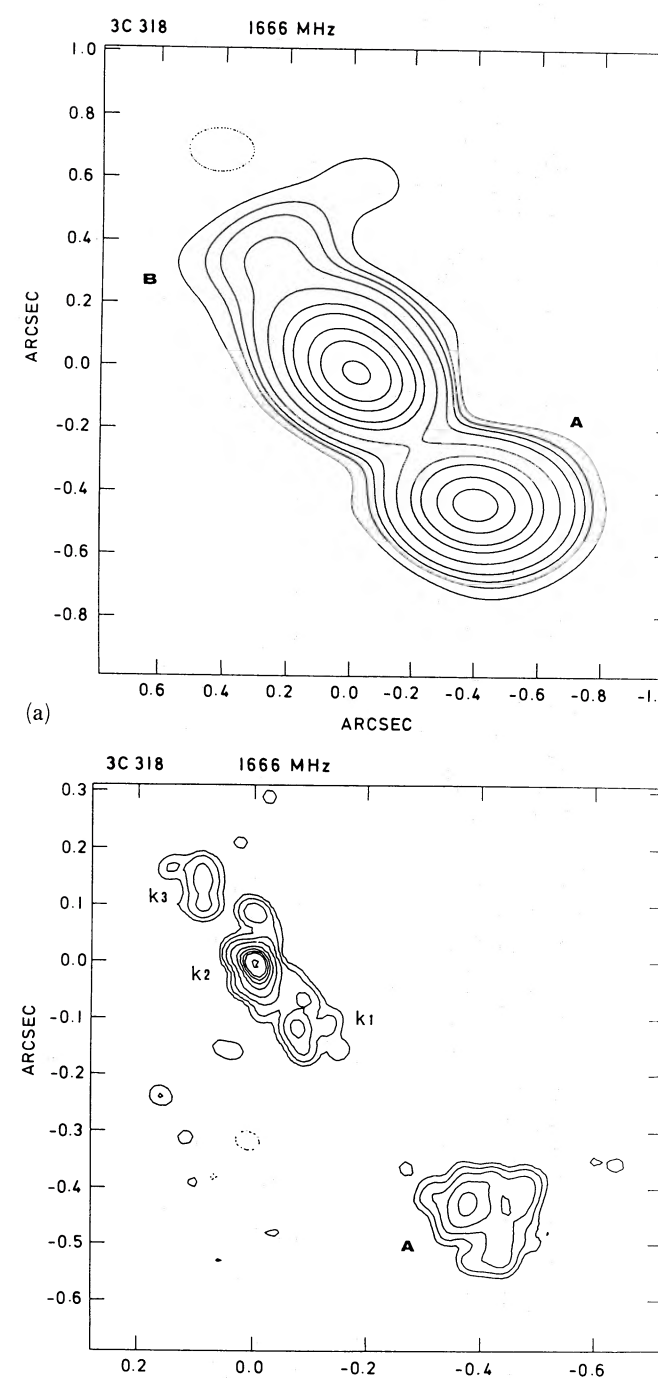


Figure 6. 3C318 (a) MERLIN map. The beam size is 275×190 mas² (pa 80°) and contours are at -8, 8, 16, 24, 40, 80, 160, 240, 400, 560 and 800 mJy beam⁻¹. (b) Combined EVN+MERLIN map. The beam size is 35×33 mas² (pa 46°) and contours are at -5.25, 5.25, 10.5, 21, 42, 84, 125, 168, 210 and 350 mJy beam⁻¹.

ARCSEC

sion, which envelops the knots at low resolution, is totally resolved out here, and the visible structure accounts for only 70 per cent of the flux density measured in this same region on the map of Fig. 1(a). Components A and B in Fig. 1(b) are the most compact, and comparison of these data with VLBI data at 610 MHz by Nan *et al.* (in preparation) indicates that A has a flat or inverted spectrum. Thus A is probably the

(b)

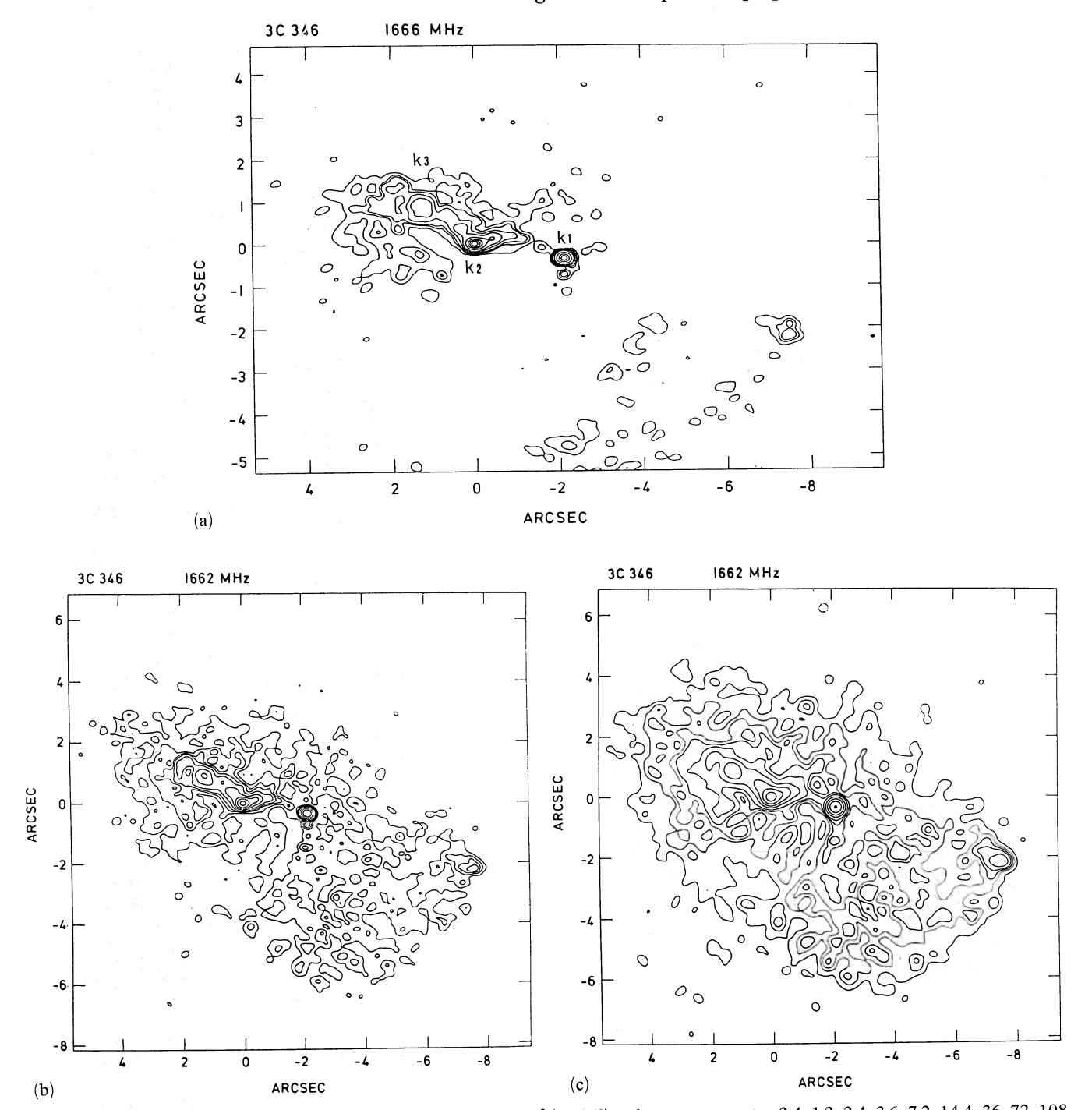


Figure 7. 3C346 (a) MERLIN map. The beam size is $250 \times 180 \text{ mas}^2$ (pa 86°) and contours are at -2.4, 1.2, 2.4, 3.6, 7.2, 14.4, 36, 72, 108 and $144 \text{ mJy beam}^{-1}$. (b) Combined VLA+MERLIN map; the beam size is $260 \times 220 \text{ mas}^2$ (pa 79°) with contours at -3, -1.5, 1.5, 3, 4.5, 6, 9, 18, 36, 72 and $144 \text{ mJy beam}^{-1}$. (c) VLA+MERLIN map, convolved to a resolution of $350 \times 350 \text{ mas}^2$ and with contours at -3, -1.5, 1.5, 3, 4.5, 6, 9, 18, 36, 72 and $144 \text{ mJy beam}^{-1}$.

source core. On this assumption we may consider the whole structure as a one-sided jet flowing to south and then bending east to join the low-brightness lobe.

The deconvolved transverse size of the jet, measured in the high-resolution map (Fig. 1b), increases from A to C reaching a width of ~15 mas (~60 pc) at 160 mas from A, then it remains constant. In the low-resolution map (Fig. 1a), the low-brightness emission around components A-F

increases the FWHM, but the overall behaviour is the same. Beyond F the faint jet may expand again at the same rate as the bright jet.

3.2 3C186

Few data are available in the literature for this source. What we have observed is the brighter component of the unequal

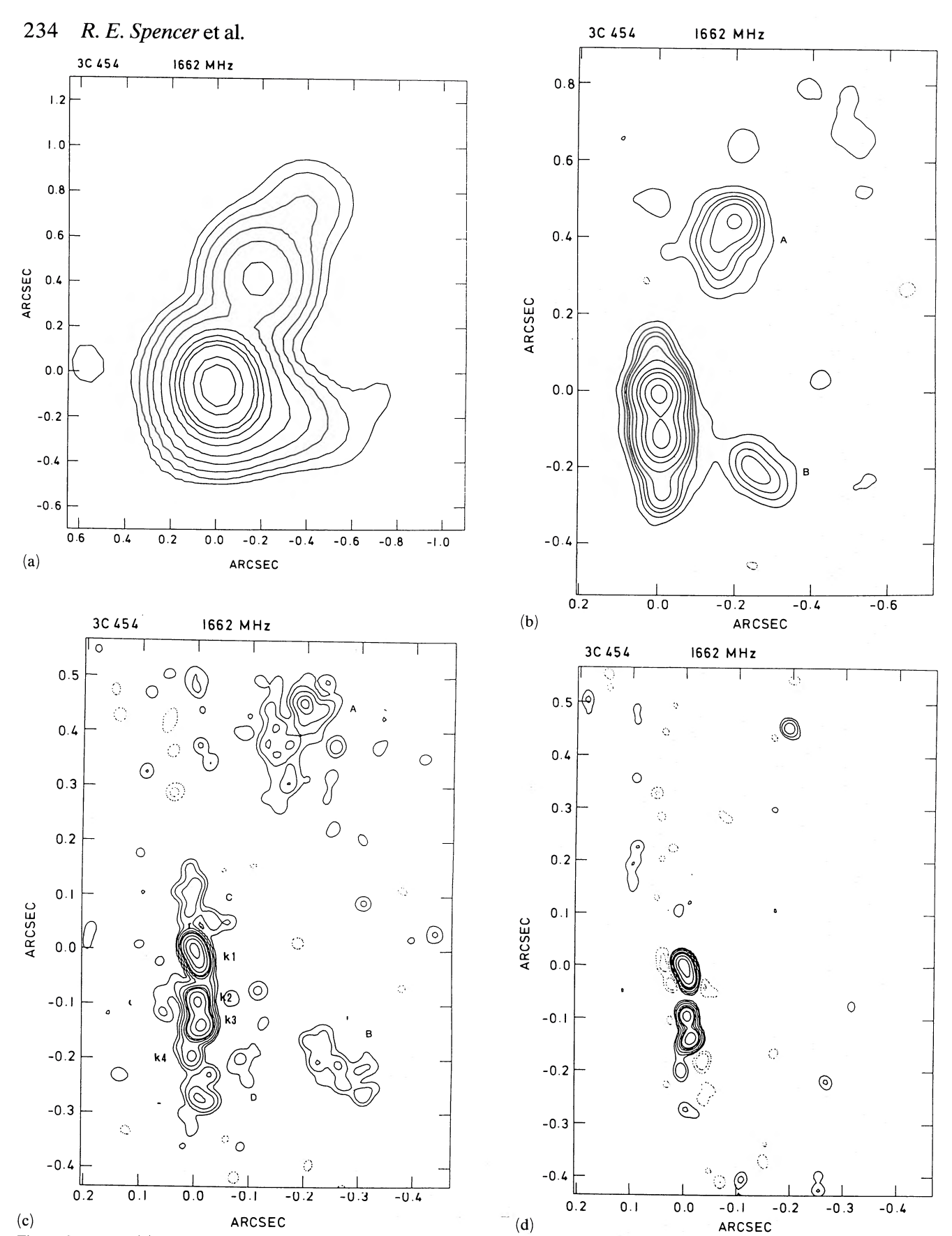


Figure 8. 3C454 (a) MERLIN map. The beam size is 250×250 mas² and the contours are at -5, 5, 10, 20, 40, 80, 160, 240, 320, 400, 640 and 800 mJy beam $^{-1}$. (b) Combined EVN + MERLIN map at a resolution of 75×75 mas² and contours at -6, 6, 12, 18, 24, 36, 60, 120, 180, 300, 450 mJy beam $^{-1}$. (c) EVN + MERLIN map at a resolution of 24×22 mas² (pa 32) with contours at -3.2, -1.6, 1.6, 3.2, 6.4, 12.8, 19.2, 25.6, 51.2, 102.4 and 204.8 mJy beam $^{-1}$. (d) EVN map. The beam size is 20×20 mas² and the contours are at -5, -2.5, 2.5, 5, 10, 20, 30, 40, 80 and 160 mJy beam $^{-1}$.

double source mapped by Schilizzi, Kapahi & Neff (1982) with the VLA at 6 cm. According to the selection criteria adopted by Fanti et al. (1985), 3C186 was included in the sample of CSS's, since the optical identification coincides with this component. The secondary component, ~130 arcsec distant at position angle (pa) 150° (Riley & Pooley 1975), accounts for only a small fraction of the total flux density and is not obviously related to the brighter one. Recent VLA observations at 20 cm (van Breugel et al. in preparation) show that this component is most likely an unrelated source and we shall not consider it further.

Higher resolution $(100 \times 100 \text{ mas}^2)$ VLA observations at 2 cm have been presented by Cawthorne *et al.* (1986). These observations show that 3C186 consists of a string of barely resolved knots, aligned in pa ~150°. The comparison of the flux densities given by Cawthorne *et al.* (1986) with the single-dish total flux density (Kühr *et al.* 1981) shows that about 30 per cent of the flux density is missing in their map. A negligible fraction of the missing flux is accounted for by the component 130 arcsec away.

A MERLIN map at 1.7 GHz, with a resolution of 162×132 mas², is shown in Fig. 2(a). The full-resolution $(28 \times 22 \text{ mas}^2)$ map (EVN + MERLIN) is given in Fig. 2(b). Here the structure can be described as an almost linear sequence of knots (a knotty jet) pointing towards two opposite lobes, symmetrically placed with respect to component k2. The southernmost component (A) displays a bend of ~ 90° with respect to the main axis of the source. This suggests that the section of component A preceding the bend may be the continuation of the jet, which reappears after a gap of ~ 600 mas (2.2 kpc) and then plunges into the lobe. The same applies to component B, and perhaps only the part of B bending to south is a lobe. The average orientations of the lobes are at $\sim 90^{\circ}$ (in A) and $\sim 60^{\circ}$ (in B) with respect to the source axis. 3C186 appears therefore as a typical S-shaped source. This is better seen in the map at intermediate resolution $(84 \times 83 \text{ mas}^2)$ of Fig. 2(c), obtained by heavily tapering the baselines longer than 4 M λ .

The two blobs k2 and k3 are oriented approximately transverse to the source main axis (Fig. 2b), and might be interpreted as transverse shocks in the jet.

The source components of the 15-GHz map by Cawthorne *et al.* (1986) are easily identified: their central component and the associated weak western extension correspond to our k1 and k2 respectively; their south-east component is the transverse lobe at A; their north-west component is our k3. The weak emission further out, not considered by Cawthorne *et al.* because it was too close to the noise, roughly corresponds to B. All these components, except k1, have a steep spectrum ($\alpha \ge 1.2$) between 0.6 GHz (Nan *et al.* in preparation) and 15 GHz, while k1 has $\alpha \sim 0.0$. We suggest that this is the source core and that the jet appears one-sided.

The fragmentation of the structure as seen in the full-resolution map prohibits reliable measurements of component parameters and the data reported in Table 3 are determined from the lower-resolution map in Fig. 2(c). From this same map, we also measured the FWHM of the jet, which appears to be constant (80-100 mas) along its entire length. The average opening angle, on the assumption that the jet is unresolved on leaving the core k1, is $\sim 8^{\circ}$ half-way along the jet.

Finally we note that lobe A contains a 'hotspot' while the

northern lobe (B) is more uniform. It is unusual that the jet points to the lobe which does not contain the brighter hot spot.

3.3 3C190

A 5-GHz map at subarcsec resolution is presented by Pearson *et al.* (1985). Here three or possibly four unresolved components appear embedded in low-brightness emission, which envelopes the whole structure.

In Fig. 3(a) we show the map obtained with the MERLIN data alone $(144 \times 128 \text{ mas}^2)$ and in Fig. 3(b) a tapered map $(230 \times 200 \text{ mas}^2)$ which shows the low-brightness emission better. These maps fully confirm the structure found by Pearson et al. (1985), and further reveal a bridge (possibly a jet) connecting the central component to the two southern ones. The spectral index between 1.7 and 5 GHz of components (A+B) and D is ~1.2, and the average spectral index of the extended low-brightness emission ~0.8. Component C has $\alpha \leq 0.5$, which suggests that this is the core. It is also the closest in position to the optical quasar (Pearson et al. 1985). The values of the spectral index are confirmed by data at 15 GHz (van Breugel et al., in preparation) and at 0.6 GHz from Nan et al. (in preparation). At this latter frequency, component C is absent (flux density < 40 MJy), indicating that it is self-absorbed below 1 GHz and confirming that it is the source core.

The high-resolution map of 3C190 (35×33 mas²) suggests a one-sided jet-like structure. At this resolution C can be split into a compact component (whose parameters are given in Table 3), which might be or contain the source core, and an extended feature which accounts for ~70 mJy. A trace of the low-brightness bridge visible in the MERLIN map can still be discerned between components C and B. It emerges from the nucleus towards the west and the bends to south by ~45° to line up with component B, possibly part of a jet. At about 1.5 arcsec from its origin (~5.6 kpc) this jetlike feature connects with the southern lobe at A. Note that this component is in the north-south direction, i.e. at an angle of $\sim 45^{\circ}$ from the last section of the jet. Examination of Fig. 3(a)-(c) suggests the following structure for 3C190: the very extended low-brightness emission of Fig. 3(a) and (b) are the lobes (L1 and L2), A and D the hotspots, the bridge and B are the jet, and C the core.

It is difficult to assess the expansion rate of the jet, due to its complexity, although it is likely that we are dealing with different expansion regimes. The angle measured at knot B (abut half-way along the jet) is $\sim 6^{\circ}$.

3.4 3C286

This source was one of the first mapped with VLBI in the late 1970's. Wilkinson & Readhead (1979), Pearson, Readhead & Wilkinson (1980) and Simon et al. (1980) produced very similar maps at 609, 1670 and 327 MHz respectively, all displaying a core-jet structure, the jet (\sim 80 mas long) being at pa \approx 130° with respect to the core. Multifrequency analysis by Simon et al. (1980) allowed estimates of the spectra of the two components to be made, although with large uncertainties: $\alpha \sim 0.3$ for the core, and $\alpha \sim 0.6$ for the jet. Phillips & Shaffer (1983) at 2.3 GHz resolved the core into two components \sim 5 mas apart; they also suggested that

the jet may have a counterpart in the north-east direction. More recently, Kus *et al.* (1988) at 1.4 GHz showed that the jet may have a greater length than previously found (~ 130 mas) and that it changes in pa from $\simeq 135$ to $\simeq 110^{\circ}$ at about 70 mas from the core. Hints of the counter-jet are visible also in their map.

At a resolution of tenths of arcsec (Spencer *et al.* 1989; Leahy *et al.*, in preparation) 3C286 is a non-linear triple source of 3.8-arcsec extension. Most of the emission is associated with the central component described above. Of the two weaker components, the eastern component is at pa $\sim 100^\circ$ and the western one is at pa -116° , i.e. roughly in the direction of the bent part of the VLBI jet. A faint extension of the central component at $\sim 23^\circ$, seen in the MERLIN and VLA maps by Spencer *et al.* (1989), the MERLIN 6-cm map of Akujor *et al.* (1991) and van Breugel *et al.* (in preparation) is consistent with this.

Our 5-GHz map $(10\times8 \text{ mas}^2\text{ resolution})$ is shown in Fig. 4(a). The core-jet structure is confirmed, and also the counter-jet found by Phillips & Shaffer (1983) is clearly visible. The surface brightness of the counter-jet is about three times fainter than that of the main jet. An unpublished map at 18 cm by Geldzahler et al. (private communication) confirms this structure. The central component of 3C286 appears, therefore, to be a two-sided jet. At 5 GHz the jet appears to 'wiggle', though this may be due to internal structure in the jet (see Zhang et al., in preparation) and it extends out to ~70 mas consistent with the other maps. We do not detect the further southern extension mapped by Kus et al. (1988). The counter-jet is only ~40 mas long.

Since our maximum baseline is $\sim 23~\text{M}\lambda$, which corresponds to a minimum fringe spacing of 9 mas, we do not have enough resolution to check whether the core is indeed double, as claimed by Phillips & Shaffer (1983). A brightness profile at pa = 47° along the jet axis (Fig. 4c) obtained from a super-resolved map with beam size $4\times4~\text{mas}^2$ (Fig. 4b) suggests that the core region could indeed be decomposed into two components, $\sim5~\text{mas}$ apart: neither of them, however, appears point-like at this resolution.

Using unpublished data at 18 cm by Geldzahler *et al.*, we derive the source spectrum along the twin jet. The spectrum is flat ($\alpha \sim 0.15$) at the source peak, then steepens gradually reaching 0.7 at blob B and probably even steeper further out, in agreement with Simon *et al.* (1980). In the counter-jet the situation is less clear, but the spectrum seems steeper than for the jet. The FWHM of the main jet reaches ~ 8 mas (30 pc) in the first 10 mas from the core, then it remains almost constant. The opening angle half-way along the jet is $\sim 15^{\circ}$. The counter-jet opens more rapidly (opening angle half-way along the jet $\sim 30^{\circ}$).

3.5 3C299

Maps at 5 and 15 GHz of this source are shown by Pearson et al. (1985) and van Breugel, Miley & Heckman (1984). They both show a slightly extended bright component, and a faint companion at ~ 11 arcsec (32 kpc) at pa = -150° , whose existence was first suspected by Riley & Pooley (1975). Recent high dynamic range VLA observations at 20 cm (van Breugel et al., in preparation) confirm this feature and show that it is extended towards the primary component, suggesting that it is indeed part of the same radio structure.

This is definitely proved by the detection, at 8.4 GHz, of a weak radio core 2.5 arcsec SW of the primary component by van Breugel *et al.* (in preparation), who present a detailed discussion of the radio and optical properties of this source. Thus the primary component is in fact the NE 'hotspot' of this very asymmetric source. Its structure, at a resolution of 30×30 mas², is shown in Fig. 5(a). The map suggests a very curved low-brightness trail on top of which a number of brighter regions are visible. The reliability of this structure is proven by the great similarity between the low-resolution map of Fig. 5(b) $(100 \times 100 \text{ mas}^2)$, the new VLA map at 15 GHz by van Breugel *et al.* (in preparation), and the MERLIN 6-cm map (Akujor *et al.* 1991). The maps are almost identical, in spite of the large frequency-range, proving also that the spectrum is uniform across the structure.

The overall structure of the hotspot of 3C299 resembles that of powerful FRII classical double sources (e.g., Laing 1989).

3.6 3C318

The source appears as a close double in the 5-GHz VLA map by Pearson *et al.* (1985), but Spencer *et al.* (1989) show that the northern component is itself a double.

At a resolution of $275 \times 190 \text{ mas}^2$, slightly higher than that of Spencer et al., component B appears oriented transverse to the general direction of the source (Fig. 6a). The MERLIN 6-cm map (Akujor et al. 1991) shows that component B has an extension to the SE, and component A is just resolved transverse to the source axis. At full resolution (35×33) mas², Fig. 6b), component B is totally resolved out, while the two other components display considerable substructure. Component A looks like a triangle, with one vertex towards the central component. The resolution is not enough to be more precise, but it seems that also on this side the source terminates in a transverse substructure, as in B. The central component contains a number of bright peaks (k1, k2, k3) which we are tempted to consider as knots in a jet, although the 'golden rule' of Bridle (1982) for the definition of a jet, i.e. a ratio 4:1 between length and width, or several blobs in a line, is not well met here. Knot k2 alone accounts for 50 per cent of the flux density of the central component (~25 per cent of the source total flux density) and is compact. Its high surface brightness and its location with respect to lobes A and B makes k2 a good candidate for the source core location. Unfortunately, information is insufficient to allow a full determination of the spectrum. The observations at 5 GHz by Pearson et al. (1985) are only able to isolate component A. Comparing this with the 15-GHz data from van Breugel et al., in preparation), we derive a spectral index $\alpha \sim 1.1$ for component A and a flatter one $(\alpha \sim 0.8)$ for the remaining structure as a whole.

If we assume that k2 contains the core, 3C318 can be described as a two-sided jet emerging from k2 which then fades before entering into the lobes. The opening angle of the visible jets is $\sim 20^{\circ}$ on both sides.

3.7 3C346

Only MERLIN and VLA data are available to us. However, because of its relatively low redshift, the linear resolution of

the MERLIN observations is comparable to that of the other CSS sources in this paper and it is appropriate, therefore, to include this source in our discussion.

A VLA map at 1.5 GHz (van Breugel *et al.*, in preparation) shows that the overall structure consists of an amorphous envelope with a number of brightness enhancements. The MERLIN 6-cm map (Akujor *et al.* 1991) just shows two bright components.

At the MERLIN resolution of $250 \times 180 \text{ mas}^2$ at 1.7 GHz (Fig. 7a), the source shows a compact component (k1) from which a jet emerges toward the east, extending with some wiggles for ~4.5 arcsec (8 kpc), where it turns sharply southwest and its brightness decreases markedly. A number of bright knots are visible along it. The width of the jet increases regularly with distance from k1 (with opening angle ~7°) while the brightness decreases, except at k2, where it increases again, and the jet bends substantially.

Unpublished MERLIN data at 408 MHz (Stannard, private communication), and VLA data at 5 and 15 GHz by van Breugel et al. (in preparation) show that component k1 is the source core, since it has a flat spectrum ($\alpha \sim 0$) between 0.4 and 15 GHz. This is the strongest core (~ 15 per cent of the total flux density at 5 GHz) in the CSS sample we are studying, and it is also relatively strong for a radio galaxy (Giovannini et al. 1988). From the same VLA data we derive spectral indices of ~ 0.44 and 0.68 for k2 and k3 respectively. The relatively flat spectra suggest that these might be locations where particle re-acceleration occurs.

The MERLIN observations shown in Fig. 7(a) miss most of the extended structure. However, this can be recovered and mapped at high resolution by carefully combining the MERLIN and the VLA data (Fig. 7b and c). The VLA observations and data calibration and reduction are described by van Breugel *et al.* (in preparation).

Since the VLA data are at a slightly different frequency (1.55 GHz) we scaled the VLA visibility amplitudes to 1.66 GHz using an average spectral index for the source of ~ 0.65 , after subtraction of the flat-spectrum component k1 from both data sets. Then, after several hybrid mapping iterations using the combined data sets to bring the visibility phases to a common reference frame, we added component k1 back to the visibilities. The final map, with a resolution of $260\times220~\mathrm{mas^2}$, was then obtained by using SDCLN task in AIPS instead of Mx, since it produces a smoother image of the low-brightness emission.

At this resolution the extended cocoon has a surface brightness of 2-3 mJy beam⁻¹, but it is still detectable. Note the hotspot to the far west, aligned with the axis k1-k3, and on the opposite side of the jet direction.

According to the statistical analysis by Fanti *et al.* (1990), 3C346 could be one of the few CSS's which are actually large-size sources shortened by projection effects. The amorphous structure might represent the radio lobes, partially overlapping because of projection (Fig. 7c, at the resolution of 0.35×0.35 arcsec²). Indeed the ratio of the total source size to transverse lobe size is small (~2), as expected for a foreshortened object. Moreover, the high brightness of the core and the jet brightness asymmetry could be produced by Doppler boosting of otherwise normal core and jet. The observed ratio of core-to-extended luminosity can be obtained from an average galaxy core (0.3 per cent, Giovannini *et al.* 1988), with a value of $\beta \cos \theta \sim 0.75$, where

 β is the speed of the jet on the mas scale and θ the angle to the line-of-sight. This implies $\beta \gtrsim 0.75$, and $\theta \lesssim 40^{\circ}$.

Also the markedly distorted structure is easy to explain as due to amplification by projection of modest intrinsic distortions. Alternatively, since the parent galaxy of 3C346 is double (van Breugel, private communication), the jet wiggles might have been caused by tidal interaction.

3.8 3C454

Pearson et al. (1985) and Cawthorne et al. (1986) present VLA and MERLIN maps of this object at several frequencies and resolutions.

Our MERLIN map (same data as Cawthorne et al. 1986) at the resolution of 250×250 mas² is presented in Fig. 8(a) for convenience. About 10 per cent of the total flux density is missing from this map, likely to be found in the extended features. In Fig. 8(b) we show a map obtained using the MERLIN and EVN data together, convolved to a resolution of 75×75 mas², comparable to that of the high-resolution maps by Cawthorne et al. (1986). The spectra computed from these maps in the range 1.7-15 GHz give $\alpha \sim 1$ and ~ 0.8 for the northern (A) and the western (B) components respectively, and $\alpha \sim 0.65$ for the central NS ridge. The MERLIN 6-cm map shows a weak component 1 arcsec N of component A.

At a higher resolution of 24 × 22 mas² (Fig. 8c), components A and B are still well visible, and the overall source shape somewhat resembles a wide angle tail (WAT), where the tails have been bent backwards, possibly by their passage from the interstellar to the intracluster medium. Note that component A contains a hotspot (23 mJy, 15×7 mas² in size), which is the only feature of component A still visible in the EVN map in Fig. 8(d) $(20 \times 20 \text{ mas}^2 \text{ resolution})$. The central ridge (Fig. 8c) shows a slightly wiggly string of knots, which, according to the definition given by Bridle (1982), could be called a jet. We do not know, however, where the core is, if it exists at all. Knot k1 can be formally split into a small-size component of ~300 mJy and a more extended one, but the resolution is insufficient to be very confident. With the present lack of information it is not possible to give a clear description of the brighter component of 3C454: we tentatively assume it to be an asymmetric straight jet, with the core located at k1, although we cannot rule out other possible sites such as in component A. The FWHM along the 'jet' is very uniform (~20 mas), and the opening angle halfway along the jet is ~11°. Note that, as in 3C186 and 3C346, the jet would then point towards the lobe which does not have a hotspot.

4 JETS IN CSS SOURCES

If we exclude 3C299, which turns out to be a larger size (~32 kpc), very asymmetric double (Section 3.5), all sources presented in this paper are jet-dominated structures. At lower angular resolution all but 3C346 are triples (Spencer et al. 1989) and the jets we see account for most of the luminosity of the central component. To have a more general overview on the occurrence of jets in CSS galaxies and quasars and on their characteristics, we have collected from the literature the available information on the resolved sources of the 3CR samples of CSS's defined by Fanti et al.

238 R. E. Spencer et al.

Table 4. Jet parameters.

Source	St ₁₈	Sj ₁₈	Scj ₁₈	Sc ₆	Brj/	Sc/	Pt		В
					Brcj	Sl	21	deg	
3C43	2670	>1130	<100	30	>25	. 050	27.71	6	par
3C48	14670	-	-	300	> 9	. 050	27.34	15	par
3C49	2310	<18	0	10	-	. 007	27.04		
3C67	2650	<20	10	<20	-	<.016	26.48		
3C119	8060	6730	1330	60	200	. 013	27.14	. 6	
3C138	8250	3870	770	250	16	. 046	27.68	8	par
3C138	19600	7000	<200	170	>40	. 069	27.84	20	
			<40	170			27.23	8	perp
3C186	1100	360			> 6	. 018		8 6	
3C190	2350	630	<20	40	> 6	. 027	27.57	ь	par
3C216	3300	900	-	500	> 5	. 324	27.22		
3C237	5580	<400		2	_	. 0006	27.69		
3C241	1400	190	<50	3	>3.4	. 0023	27.80		
3C268.3	3250			<20	/3.4 ~	<.012	26.73		
3C286.3	14040		<100 13570		2.8	. 012	27.94	15	
3C287	6240	1337		900 240	2.0	. 047	27.82	15	perp
30287	6240		_	240	_	. 04.7	21.02		
3C298	4870	>740	<70	220	>6	. 058	28, 17	5?	par
3C303.1	1480	<12		<5	_	<.010	26.14		
3C305.1	1450	<130		<6	_	<.006	27, 38		
3C309.1	6600	3300	_	700	>40	. 16	27.75	15	par
3C318	2190	165	125	<90	1.6	<.07	27.18	20	par
00010	2270	100	100	.,,	1.0		220	20	.
3C343	4310	_	_	-	-	-	27.65		
3C343.1	3890	<22	20	<60	-	<.02	27.41		
3C346	3400	800	<50	220	>15	. 147	26.00	7	par
3C380	12700		-	1000	_	. 38	27.78	<15	
3C454	1900	950	~65	<200	7.7	<. 11	27.75	11	

Columns: 1 – source name; 2 – St, flux density at 18 cm; 3, 4 – Sj, Scj, flux densities of jet and counter-jet, at 18 cm; 5 – Sc, core flux density at 6 cm; 6 – Brj/Brc, jet to counter-jet brightness ratio; 7 – Sc/Sl, ratio of core to extended flux density, corrected for k term, at 5 GHz; 8 – Pt, log of total radio luminosity at 21 cm (W Hz $^{-1}$); 9 (th), average jet opening angle; 10 – B, magnetic field (B) orientation in the jet(s); par – B parallel to the jet; perp – B perpendicular to the jet.

(1985). The definition of a jet may be somewhat uncertain, but if we take the operative definition given by Bridle (1982) we find that it applies satisfactorily to most of the sources we are considering.

In Table 4 we give the flux density (or an upper limit to it) of jets and cores and, when a jet is detected, an estimate of the ratio of the surface brightness in the jet to that in the counter-jet (or upper limit). When no jet is visible, upper limits to the flux density have been computed as 2 rms noise × lobe separation (in units of beam size, assuming that the jet is unresolved or only slightly resolved transverse to its axis). This is usually a high upper limit, since it assumes that the jet extends both ways from the core to the lobes. Upper limits to the flux density of undetected counter-jets have been estimated in a similar fashion. It is not possible to determine for all the sources the complete set of parameters, so the following discussion will deal with an incomplete, but, we believe, still representative, sample of jets in CSS's.

Table 4 shows that bright jets are present in 11 of the 15 QSS listed (73 per cent) and in three of the 10 galaxies (30 per cent). Two more quasars (3C48, 3C380) have such a complex structure that it is difficult to say which part of the structure is the jet, although it seems that for 3C48 the jet accounts for most of the structure (Wilkinson *et al.* 1990).

4.1 Jet collimation

The jets appear generally well collimated; the average opening angle, measured half-way along the jet, is usually 5-15°

(median value ~ 8°), similar to the jets in large-scale, 'powerful' sources (Bridle & Perley 1984).

A number of jets in CSS sources show non-uniform expansion. In addition to 3C138, studied by Fanti *et al.* (1989), several cases are presented in this paper (e.g. 3C286). A general behaviour seems to be a larger spreading rate close to the core, followed by some recollimation. The initial opening angle can be relatively large but the average opening angle is small, due to the extent of the collimation regime. Recollimation suggests that the effects of the external medium are not negligible, and the presence of the interstellar gas is an important factor.

4.2 Polarization

Integrated polarization information at high frequency on these jets (typically at 5 and 15 GHz from VLA; van Breugel et al. 1984, and van Breugel et al., in preparation) is available for several sources. The magnetic field orientations, inferred by assuming negligible Faraday rotation at these high frequencies, are also included in Table 4.

In most cases the magnetic fields are aligned parallel to the jet. This is similar to the innermost regions of the jets in large-scale FRII radio sources (Bridle 1982). However, in 3C147, 190 and 286, the magnetic field is transverse to the jet.

4.3 Curvature and bending

The jets show a large variation in radio structure. Most jets exhibit wiggling and bending (3C138, 286, 346), with extreme cases such as 3C43, 119, 287, 309.1 and 454.

What causes the extreme structures is impossible to say in the absence of other information. Current ideas are that the jet strikes dense clouds in the gas region surrounding the quasar (galaxy) nucleus (e.g., van Breugel *et al.* 1988). Sharp bends, such as in 3C43 or 3C454, are difficult to explain by geometric projection only of a moderately distorted jet. More regular bending or wiggling could be due to precession (see the discussion on 3C138, Fanti *et al.* 1989; 3C119, Fanti *et al.* 1986; Nan *et al.*, in preparation).

4.4 Brightness enhancements in the jets

In most jets the brightness distribution is dominated by prominent knots, but there may be an underlying jet emission of lower brightness. There does not appear to be any clear rule for the location of the knots along the jet. In a few cases the knots are found where the jet trajectory sharply bends (e.g., 3C43, 3C346). This may be explained as the result of shocks against a highly inhomogeneous interstellar medium. Alternatively it might be due to Doppler boosting, when the bending causes the (relativistic) jet flow to approach the line-of-sight. Note that there are cases, e.g. 3C119 and 3C454, where a sharp bend in the jet corresponds to a significant decrease in brightness. This can be consistent with beaming effects if the jet is moving away from the observer.

In 3C186 two blobs are clearly extended transverse to the jet axis, as is seen in the SE jet in 3C236 (Schilizzi *et al.* 1988) and in the M87 jet (knot A; Biretta, Owen & Hardee

1983). They could originate from compression of the magnetic field in a transverse shock resulting from interaction with the external medium. Such an explanation may apply also to other knotty jets in the sample. There is, however, no obvious relation between the orientation of the knots and the jet axis in these cases. The presence of elongation in directions away from that of the jet is perhaps evidence for interaction with an inhomogeneous interstellar medium rather than brightening by strong beaming effects.

Brightness asymmetry 4.5

Except for 3C286 and 3C318, the jets in this sample are asymmetric according to the definition by Bridle & Perley (1984) (brightness ratio > 4).

Counter-jets much fainter than the main jet are detected in 3C138 (Fanti et al. 1989), and, possibly, in 3C454. In 3C119 it is uncertain whether part of the structure can be interpreted as a counter-jet or whether the whole structure is due to a single, extremely curved, jet. For the remaining nine sources, only upper limits can be given to the flux density of a possible counter-jet.

In order to quantify the brightness asymmetries, we take, as an indicator of the average surface brightness of the jet, the arithmetic mean of the three highest peaks in the jet. Furthermore we assume an upper limit of 5 times the rms noise level for the surface brightness of any undetected counter-jet.

From the distribution (not shown) of brightness ratios and upper limits we deduce a lower limit of 8:1 to the median value of the asymmetry ratio. Such asymmetries could be due to a flip-flop mechanism (Rudnick 1981), in which the jet points alternately to either lobe. In this hypothesis we might expect differences in the age of the two outer lobes, if the flip-flop occurs on time-scales comparable to the radiative lifetime. However, the spectral indices of the two lobes are very similar (Fanti et al. 1990), which suggests that the ages of the radiating electrons in each lobe are not greatly different. So it seems that the flip-flop mechanism is not applicable unless the flip-flop occurs on a time-scale which is less than the radiation lifetime, in which case we would not expect to see the large brightness asymmetries observed.

Asymmetry in jets is often believed to result from Doppler boosting in a symmetric jet aligned close to the line-of-sight. The sources of our sample can be used to derive ranges of values for the orientation and for the speed of the jet, on the usual assumptions that the jet emission is intrinsically symmetric and that the jet/counter-jet brightness ratio, produced by relativistic boosting, is given by $R = (1 + \beta \cos \theta/1 - \beta \cos \theta)$ θ)^{2+a}. If CSS's are randomly oriented in the sky, as seems plausible (Fanti et al. 1990), the median angle to the line-ofsight is 60°; for an average spectral index α of 0.8, a median $\beta \ge 0.7$ is sufficient to produce the observed asymmetry.

Jet asymmetries could therefore be due to relativistic beaming, without requiring highly relativistic flow velocities and without introducing any orientation bias in the sample. For instance, the jet/counter-jet brightness ratio in 3C286 can be obtained for $\beta > 0.5$ and angles to the line-of-sight >60°. Nevertheless, one should keep in mind the case of 3C138, where a small one-sided pc-scale jet is visible in the direction opposite to the one-sided kpc-scale jet (Fanti et al. 1989). This example shows that an interpretation in terms of Doppler effects may be too simplistic.

4.6 Core and jet luminosity

Cores are detected in 68 per cent of the objects (13 QSS and 4 galaxies) and are generally weak with respect to the total flux density, with a fractional luminosity comparable to that of large-scale extended radio sources. This is consistent with the hypothesis of a random orientation of CSS's in the sky.

Fig. 9 shows a plot of the ratio of core flux density (Sc) to total flux density (St), versus the ratio of jet flux density (Sj) to St. As is already known, CSS quasars have stronger cores and stronger jets than CSS galaxies and the two categories of object are well separated in this plot. We note, however, that of the two galaxies with strong jets (3C346 and 318) at least the first has also a strong core and falls in the region occupied by quasars. This may be weak evidence that stronger jets are related to the presence of the stronger cores, independent of the optical identification.

CONCLUSIONS

- (i) This paper concludes a VLBI, MERLIN and VLA study began in 1981 on properties of a sample of 3CR CSS sources. The sources in the sample, summarized in Table 1, now have a complete set of maps at 1.6 GHz with a linear resolution of ≤ 100 pc.
- (ii) The use of combined mapping techniques (EVN+MERLIN or VLA+MERLIN) on the eight sources reported here have enabled images to be produced with high dynamic range. The relationship between low-brightness extended regions and high-brightness jets can be seen more

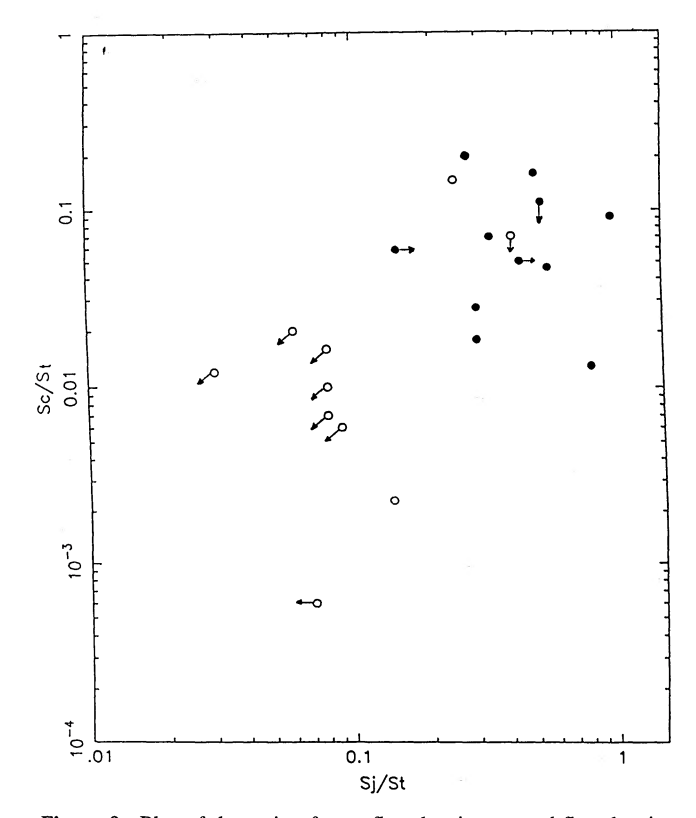


Figure 9. Plot of the ratio of core flux density to total flux density, versus the ratio of jet flux density to total flux density. O indicates galaxies, • indicates quasars.

clearly than on previous maps from the EVN or MERLIN alone.

(iii) The eight sources show the presence of bright jets which account for a large fraction of the source luminosity. Most of these jets are one-sided and show conspicuous brightness enhancements and bending. Their expansion regime seems to consist of different phases with different spreading rates. The average 'opening angle', however, is in general small ($\leq 10^{\circ}$). These properties indicate that interaction with an external medium is dynamically important, while the brightness asymmetries found are consistent with mildly relativistic jet velocities.

ACKNOWLEDGMENTS

We thank the staff at the Caltech and MPI VLBI processors for their help in correlating the VLBI recordings, and Dr G. Pooley and the staff at MRAO Cambridge for their assistance with the 18-m telescope.

The VLA is a facility of the National Radio Astronomy Observatory which is operated by Associated Universities Inc. under contract to the National Science Foundation.

REFERENCES

- Akujor, C. E., Spencer, R. E., Zhang, F. J., Davis, R. J., Browne, I. W. A. & Fanti, C., 1991. Mon. Not. R. astr. Soc., 250, 119.
- Barthel, P. D., Pearson, T. J. & Readhead, A. C. S., 1988. *Astrophys. J.*, **329**, L51.
- Biretta, J. A., Owen, F. N. & Hardee, P. E., 1983. Astrophys. J., 274, L27.
- Bridle, A. H., 1983. Extragalactic Radio Sources, IAU Symp. No. 97, p. 121, eds Heeschen, D. S. & Wade, C. M., Reidel, Dordrecht.
- Bridle, A. H. & Perley, R. A., 1984. Ann. Rev. Astr. Astrophys., 22, 319.
- Cawthorne, T. V., Scheuer, P. A. G., Morison, I. & Muxlow, T. W. B., 1986. Mon. Not. R. astr. Soc., 219, 883.
- Cohen, M. H. et al., 1975. Astrophys. J., 201, 249.
- Cornwell, T. J. & Wilkinson, P. N., 1981. Mon. Not. R. astr. Soc., 196, 1067.
- Cornwell, T. J. & Wilkinson, P. N., 1983. In: *Indirect Imaging*, p. 207, ed. Roberts, J. A., Cambridge University Press, Cambridge.
- Fanti, C., Fanti, R., Parma, P., Schilizzi, R. T. & van Breugel, W. J. M., 1985. Astr. Astrophys., 143, 292.
- Fanti, C., Fanti, R., Schilizzi, R. T., Spencer, R. E. & van Breugel, W. J. M., 1986. Astr. Astrophys. J., 170, 10.
- Fanti, R., Fanti, C., Schilizzi, R. T., Spencer, R. E., Nan Rendong, Parma, P., van Breugel, W. J. M. & Venturi, T., 1990. Astr. Astrophys., 231, 333.

- Fanti, C., Fanti, R., Parma, P., Venturi, T., Schilizzi, R. T., Nan Rendong, Spencer, R. E., Muxlow, T. W. B. & van Breugel, W. J. M., 1989. Astr. Astrophys., 217, 44.
- Giovannini, G., Feretti, L., Gregorini, L., Parma, P. & Zamorani, G., 1988. Astr. Astrophys., 199, 73.
- Jenkins, C. J., Pooley, G. G. & Riley, J. M., 1977. Mem. R. astr. Soc., 84, 61.
- Kühr, H., Witzel, A., Pauliny-Toth, I. I. K. & Nauber, U., 1981. Astr. Astrophys. Suppl., 45, 367.
- Kus, A. J., Marecki, A., Neff, S., van Ardenne, A. & Wilkinson, P. N., 1988. The impact of VLBI on Astrophysics and Geophysics, IAU Symp. No. 129, p. 129, eds Reid, M. J. & Moran, J. M., Kluwer, Dordrecht.
- Laing, R., 1989. In: Hot Spots in Extragalactic Radio Sources, Lecture Notes in Physics, p. 27, eds Meisenhemer, K. & Roser, H.-J., Springer-Verlag, Berlin.
- Muxlow, T. W. B., Junor, W., Spencer, R. E., Simon, R., Benson, J. & Reid, M., 1988. The Impact of VLBI on Astrophysics and Geophysics, IAU Symp. No. 129, p. 131, eds Reid, M. J. & Moran, J. M., Kluwer, Dordrecht.
- Pearson, T. J., Perley, R. A. & Readhead, A. C. S., 1985. *Astr. J.*, **90**, 738
- Pearson, T. J., Readhead, A. C. S. & Wilkinson, P. N., 1980. Astrophys. J., 236, 714.
- Phillips, R. B. & Shaffer, D. B., 1983. Astrophys. J., 271, 32.
- Riley, J. M. & Pooley, G. G., 1975. Mem. R. astr. Soc., 80, 105.
- Rudnick, L., 1981. IAU Symp. No. 97, p. 47, eds Heeschen, D. S. & Wade, C. M., Reidel, Dordrecht.
- Schilizzi, R. T., Kapahi, V. K. & Niff, S. G., 1982. J. Astrophys. Astr., 3, 173.
- Schilizzi, R. T., Skillman, E. D., Miley, G. K., Barthel, P. D., Benson, J. M. & Muxlow, T. W. B., 1988. The impact of VLBI on Astrophysics and Geophysics, IAU Symp. No. 129, p. 131, eds Reid, M. J. & Moran, J. M., Kluwer, Dordrecht.
- Simon, R. S., Readhead, A. C. S., Moffett, A. T., Wilkinson, P. N. & Anderson, B., 1980. *Astrophys. J.*, **236**, 707.
- Spencer, R. E., McDowell, J. C., Charlesworth, M., Fanti, C., Parma, P. & Peacock, J. A., 1989. *Mon. Not. R. astr. Soc.*, **240**, 657.
- van Breugel, W. J. M., Miley, G. K. & Heckman, T., 1984. Astr. J., 89, 5.
- van Breugel, W. J. M., Nan Ren-dong, Schilizzi, R. T., Fanti, C. & Fanti, R., 1988. *The impact of VLBI on Astrophysics and Astronomy, IAU Symp. No. 129*, p. 115, eds Reid, M. J. & Moran, J. M., Kluwer.
- Wilkinson, P. N. & Readhead, A. C. S., 1979. Astrophys. J., 232, 365.
- Wilkinson, P. N., Booth, R. S., Cornwell, T. J. & Clark, R. R., 1984b.
 Nature, 308, 619.
- Wilkinson, P. N., Spencer, R. E., Readhead, A. C. S., Pearson, T. J. & Simon, R. S., 1984a. VLBI and Compact Radio Sources, IAU Symp. No. 110, p. 25, eds Fanti, R., Kellermann, K. I. & Setti, G., Reidel, Dordrecht.
- Wilkinson, P. N., Tzioumis, A. K., Akujor, C. E., Benson, J. M., Walker, R. C. & Simon, R. S., 1990. In: *Parsec-Scale Radio Jets*, p. 152, eds Zensus, J. A. & Pearson, T. S., Cambridge University Press, Cambridge.